

Provided for non-commercial research and education use.  
Not for reproduction, distribution or commercial use.



This article appeared in a journal published by Elsevier. The attached copy is furnished to the author for internal non-commercial research and education use, including for instruction at the authors institution and sharing with colleagues.

Other uses, including reproduction and distribution, or selling or licensing copies, or posting to personal, institutional or third party websites are prohibited.

In most cases authors are permitted to post their version of the article (e.g. in Word or Tex form) to their personal website or institutional repository. Authors requiring further information regarding Elsevier's archiving and manuscript policies are encouraged to visit:

<http://www.elsevier.com/copyright>



Contents lists available at ScienceDirect

# Journal of Quantitative Spectroscopy & Radiative Transfer

journal homepage: [www.elsevier.com/locate/jqsrt](http://www.elsevier.com/locate/jqsrt)

## Photoionization and electron–ion recombination of Cr I

Sultana N. Nahar\*

Department of Astronomy, The Ohio State University, Columbus, OH 43210, USA

### ARTICLE INFO

**Article history:**

Received 28 January 2009

Received in revised form

21 April 2009

Accepted 29 April 2009

**PACS:**

31.15.vj

32.80.Fb

32.80.Zb

**Keywords:**

Photoionization and electron–ion recombination

Cr I

ISM

### ABSTRACT

Using the unified method, the inverse processes of photoionization and electron–ion recombination are studied in detail for neutral chromium, ( $\text{Cr I} + h\nu \leftrightarrow \text{Cr II} + e$ ), for the ground and excited states. The unified method based on close-coupling approximation and R-matrix method (i) subsumes both the radiative recombination (RR) and dielectronic recombination (DR) for the total rate and (ii) provides self-consistent sets of photoionization cross sections  $\sigma_{PI}$  and recombination rates  $\alpha_{RC}$ . The present results show in total photoionization of the ground and excited states an enhancement in the background at the first excited threshold,  $3d^4 4s^5 D$  state of the core. One prominent phot-excitation-of-core (PEC) resonance due to one dipole allowed transition ( ${}^6S - {}^6P^o$ ) in the core is found in the photoionization cross sections of most of the valence electron excited states. Structures in the total and partial photoionization, for ionization into various excited core states and ground state only, respectively, are demonstrated. Results are presented for the septet and quintet states with  $n \leq 10$  and  $l \leq 9$  of Cr I. These states couple to the core ground state  ${}^6S$  and contribute to the recombination rates. State-specific recombination rates are also presented for these states and their features are illustrated. The total recombination rate shows two DR peaks, one at a relatively low temperature, at 630 K, and the other around 40,000 K. This can explain existence of neutral Cr in interstellar medium. Calculations were carried out in LS coupling using a close-coupling wave function expansion of 40 core states. The results illustrate the features in the radiative processes of Cr I and provide photoionization cross sections and recombination rates with good approximation for this astrophysically important ion.

© 2009 Elsevier Ltd. All rights reserved.

### 1. Introduction

Neutral Chromium, Cr I, has been studied by many investigators largely because of its presence in astronomical objects. Lines of Cr I has been observed recently in interstellar medium toward HD 72127AB [1]. Among a number of experiments, low energy photoionization features of Cr I were observed by Huber et al. [2] while very high energy photo-absorption features were observed by Cooper et al. [3]. There has been less theoretical study on Cr I compared to various experiments. Much of the study is concentrated to small energy region and for the ground or very few excited states. For example, Dolmatov studied [4] using spin-polarized random phase approximation the two states  ${}^7S$  and  ${}^5S$  of the ground configuration and found that  ${}^5S$  photoionization cross section is much higher than that of the ground  ${}^7S$ . The study does not include resonant structures. In contrast to the number of studies on photo-absorption, no report on electron–ion recombination process for this atomic system is not available.

\* Tel.: +1614 292 1888; fax: +1614 292 2928.

E-mail address: [nahar@astronomy.ohio-state.edu](mailto:nahar@astronomy.ohio-state.edu)

The atomic properties for Cr I are strongly perturbed by electron–electron correlations as the atom is neutral and holds a large number of electrons. This makes it difficult to represent the atom with an accurate wave function. The present study aims to study in detail with autoionizing resonances the inverse processes of photoionization and recombination of Cr I for the ground and excited states using the *ab initio* unified method and provide results of good approximation.

## 2. Theory

Cr I is studied using the unified method [5,6] which is based on the close-coupling (CC) approximation and R-matrix method implemented under the Opacity Project (OP) [7] and the Iron Project (IP) [8]. A brief outline of the theory relevant to the present calculations is given below.

In the CC approximation, the atomic system of an ion and an interacting electron is represented by the ‘target’ or the ‘core’ of  $N$  electrons interacting with the  $(N + 1)$ th electron. The  $(N + 1)$ th electron may be bound or in the continuum depending on its energy ( $E$ ) being negative or positive. The total wavefunction,  $\Psi_E$ , of the  $(N + 1)$  electrons system in a symmetry  $SL\pi$  is expressed by an expansion,

$$\Psi_E(e + ion) = A \sum_i \chi_i(ion)\theta_i + \sum_j c_j \Phi_j, \quad (1)$$

where the target ion eigenfunction,  $\chi_i$ , is coupled with the  $(N + 1)$ th electron function,  $\theta_i$ . The sum is over the ground and excited core states. The  $(N + 1)$ th electron with kinetic energy  $k_i^2$  is in a channel labeled as  $S_i L_i \pi_i k_i^2 \ell_i (SL\pi)$ . In the second sum, the  $\Phi_j$ s are bound channel functions of the  $(N + 1)$ -electrons system that account for short range correlation and the orthogonality between the continuum and the bound electron orbitals.

The Hamiltonian of the  $(N + 1)$ -electrons system is given by

$$H_{N+1} = \sum_{i=1}^{N+1} \left\{ -\nabla_i^2 - \frac{2Z}{r_i} + \sum_{j>i}^{N+1} \frac{2}{r_{ij}} \right\} + H_{N+1}^{mass} + H_{N+1}^{Dar} + H_{N+1}^{so}, \quad (2)$$

where the first sum is the non-relativistic Hamiltonian and the last three terms are relativistic corrections; the mass correction ( $H^{mass}$ ), Darwin ( $H^{Dar}$ ) and spin–orbit interaction ( $H^{so}$ ), respectively (e.g. [9]). Present calculations are carried out in LS coupling, that is, no relativistic correction is considered. Substitution of  $\Psi_E(e + ion)$  in the Schrodinger equation

$$H_{N+1} \Psi_E = E \Psi_E, \quad (3)$$

introduces a set of coupled equations that are solved using the R-matrix method. The solution is a continuum wavefunction,  $\Psi_F$ , for an electron with positive energies ( $E > 0$ ), or a bound state,  $\Psi_B$ , at a negative total energy ( $E \leq 0$ ). The complex resonant structures in photoionization or recombination result from couplings between the continuum channels and bound channels at electron energies  $k_i^2$  corresponding to autoionizing states of the Rydberg series,  $S_i L_i \pi_i \nu \ell$  where  $\nu$  is the effective quantum number, belonging to excited target or core state  $S_i L_i \pi_i$ .

Transition matrix elements for photoionization,  $\langle \Psi_B || \mathbf{D} || \Psi_F \rangle$  where  $\mathbf{D} = \sum_i r_i$  is the dipole operator and the sum is over the number of electrons, are obtained from the bound and continuum wavefunctions. The transition matrix element is reduced to generalized line strength as

$$\mathbf{S} = |\langle \Psi_f || \mathbf{D} || \Psi_i \rangle|^2 = \left| \left\langle \psi_f \left| \sum_{j=1}^{N+1} r_j \right| \psi_i \right\rangle \right|^2, \quad (4)$$

where  $\Psi_i$  and  $\Psi_f$  are the initial and final state wavefunctions. The photoionization cross section ( $\sigma_{PI}$ ) is proportional to the generalized line strength

$$\sigma_{PI} = \frac{4\pi^2}{3c} \frac{1}{g_i} \omega \mathbf{S}, \quad (5)$$

where  $g$  is the statistical weight factor of the bound state and  $\omega$  is the incident photon energy. The details of the R-matrix method in the CC approximation for photoionization can be found in [10,11].

The unified method considers the inverse nature of electron–ion recombination and photoionization. It obtains recombination cross sections,  $\sigma_{RC}$ , from *partial* photoionization cross section by using the principle of detailed balance or Milne relation

$$\sigma_{RC} = \sigma_{PI} \frac{g_i}{g_j} \frac{h^2 \omega^2}{4\pi^2 m^2 c^2 \nu^2}, \quad (6)$$

where  $g_j$  is the statistical weight factor of the recombined state and  $\nu$  is the photoelectron velocity. The recombining ion is assumed to be in the ground state. The detailed autoionizing structures in photoionization cross sections are integrated for recombination cross sections through the Milne relations. Hence the sum corresponds to inclusion of both the radiative recombination (RR) and dielectronic recombination (DR) in an unified and *ab initio* manner.

The state-specific recombination rate coefficient of state  $i$  is obtained by averaging the recombination cross sections over the Maxwellian electron distribution,  $f(v) = (4/\sqrt{\pi})(m/2kT)^{3/2}v^2e^{-mv^2/2kT}$ , as

$$\alpha_R(i; T) = \int_0^\infty v f(v) \sigma_{RC}(i) dv. \quad (7)$$

The total recombination rate can be obtained from the sum of these individual rates, that is,  $\alpha_R(T) = \sum_i \alpha_R(i, T)$  where the sum is over infinite number of recombined states.

The highly excited states lie close to each other and the resonances become narrower while the background is low. The unified method divides the infinite number of recombined states into two groups: group (A) states with  $n \leq n_o$ , and group (B) states with  $n_o < n \leq \infty$ , where  $n_o \sim 10$ . The recombination rates coefficients of group (A) states are obtained from the photoionization cross sections as described above. Recombination into group (B) states, which are in a small energy range, is dominated by DR via high- $n$  resonances while the background recombination, that is, RR is negligibly small. Bell and Seaton [12] developed a treatment of the DR process based on quantum defect theory and close-coupling approximation and obtained an expression for the averaged DR probability,  $\langle P_n^{SL\pi}(DR) \rangle$ , where  $n$  denotes the entrance channel. The work was extended by Nahar and Pradhan [6] for DR calculations. The DR probability is given by [12],

$$P_n(DR) = (1 - \mathcal{S}_{ee}^\dagger \mathcal{S}_{ee})_n, \quad (8)$$

where  $\mathcal{S}_{ee}$  is the electron scattering matrix including radiation damping. In the energy region of these states below each target state, the electron–electron scattering matrix is partitioned into submatrices,  $\chi_{oo}, \chi_{oc}, \chi_{co}, \chi_{cc}$ , where ‘o’ denotes the open and ‘c’ denotes the closed channels.  $\chi_{cc}$  is diagonalized as  $\tilde{\chi}_{cc} = \mathbf{N}^\dagger \chi_{cc} \mathbf{N}$  where  $\mathbf{N}$  is complex. With  $\mathbf{N}$ , we define  $\tilde{\chi}_{co} = \mathbf{N}^\dagger \chi_{co}$ ,  $\tilde{\chi}_{oc} = \chi_{oc} \mathbf{N}$ . Bell and Seaton obtained [12]

$$\langle P_\alpha(DR) \rangle = G \sum_{\gamma, \gamma'} \frac{\tilde{\chi}_{\alpha\gamma} \tilde{\chi}_{\gamma'\alpha}^* (\mathbf{N}^\dagger \mathbf{N}^*)_{\gamma\gamma'}}{G + 1 - \tilde{\chi}_{\gamma\gamma} \tilde{\chi}_{\gamma'\gamma'}^*}, \quad (9)$$

where  $G(v) = g(v)^2 - 1$ ,  $g(v) = \exp(\pi v^3 A_r / z^2)$ ,  $A_r$  is the sum of the radiative decay probabilities for the available decay routes from a given excited state of the target ion,  $v$  is the effective quantum number associated with the resonance series,  $z$  is the ion charge, and the summations go over the closed channels  $\gamma\gamma'$  contributing to DR.

For computational purposes,  $\langle P_\alpha(DR) \rangle$  needs further expansion, as was carried out by Nahar and Pradhan [6]. Using some algebra, the expression can be reduced to direct and interference terms as [6]

$$\langle P_\alpha(DR) \rangle = G(v) \left[ \sum_\gamma \frac{|\tilde{\chi}_{\alpha\gamma}|^2 \sum_i |\mathbf{N}_{i\gamma}|^2}{G(v) + 1 - |\chi_{\gamma\gamma}|^2} + 2 \sum_{\gamma \neq \gamma'} \text{Re} \left( \frac{\tilde{\chi}_{\alpha\gamma} \tilde{\chi}_{\gamma'\alpha} \sum_i \mathbf{N}_{i\gamma} \mathbf{N}_{i\gamma'}}{G(v) + 1 - \chi_{\gamma\gamma} \chi_{\gamma'\gamma'}} \right) \right], \quad (10)$$

where the summation over  $i$  goes through all the closed channels. The DR probability from the general scattering matrix, which includes the radiation damping, can also be used for detailed structures. However, the general expression given by Bell and Seaton causes numerical instability. Using the diagonalizing matrix,  $\mathbf{N}$ , a numerical stable form can be obtained. Starting from the unitarity condition of the general scattering matrix,  $P_\alpha$  can be written in terms of the matrix elements as [6]

$$P_\alpha = G(v) \sum_\gamma \left\{ \left( \sum_{\gamma'} \tilde{\chi}_{\alpha\gamma'} \mathbf{N}_{\gamma\gamma'} \right) \left[ \frac{1}{\chi_{\gamma\gamma} - g(v) \exp(-2\pi i v)} \right] \left[ \frac{1}{\chi_{\gamma\gamma}^* - g(v) \exp(+2\pi i v)} \right] \left( \sum_{\gamma'} \tilde{\chi}_{\gamma'\alpha}^* \mathbf{N}_{\gamma\gamma'}^* \right) \right\}. \quad (11)$$

This is a precise treatment for the DR process for its an ab initio nature and inclusion of interference of channels compared to other existing methods, such as, isolated resonance approximation or Burgess formula.

The DR collision strengths,  $\Omega(DR)$ , is obtained as

$$\Omega(DR) = \sum_{SL\pi} \sum_n \frac{1}{2} (2S + 1)(2L + 1) P_n^{SL\pi}(DR). \quad (12)$$

Calculations for  $\Omega(DR)$  are carried out in the CC approximation using the same wavefunction expansion used for photoionization cross sections. The recombination cross section  $\sigma_{RC}$  is related to  $\Omega(DR)$  as,

$$\sigma_{RC}(DR) = \frac{\pi}{g_i k^2} \Omega(DR) a_o^2. \quad (13)$$

$\Omega(DR)$  is summed over all contributing symmetries  $SL\pi$ . The total DR contributions of  $n > 10$  states is usually much smaller than that for  $n < 10$  states except at the DR peak where it can still be smaller but of the same order. The RR-type ‘background’ contributions from the high- $n$  group (B) states,  $n_o < n \leq \infty$ , to the total recombination rate are included in hydrogenic approximation [13]. These contributions are usually negligible except at very low temperatures where electron energies are not high enough for core excitations.

Experimental set-ups are able to measure recombination spectra for rates with electron energy. Such spectra can be produced from unified total recombination cross sections

$$\alpha_R(E) = \nu \sigma_{RC}(E), \tag{14}$$

where  $\nu$  is the photoelectron energy.  $\alpha_R(E)$ , being proportional directly to  $\sigma_{RC}(E)$ , reveals detailed resonant features in electron–ion recombination spectrum and is of considerable interest to experimental facilities.

### 3. Computations

Computations for photoionization and electron–ion recombination are carried out in a number of steps. The initial step is to obtain the target or core wave functions from atomic structure calculations. The code SUPERSTRUCTURE [14], which employs Thomas–Fermi–Dirac potential to generate one–electron orbitals, was used to obtain wave function of core Cr II by optimizing a set of 14 configurations listed in Table 1. The lowest 40 states of Cr II, given in Table 1, were selected for the wave function expansion of Cr I. For accurate resonance positions, observed energies from NIST compilation [15] were used. The fine structure energies in NIST table were averaged statistically to obtain the LS term energies in Table 1.

The computations for photoionization cross sections of Cr I were carried out using the R-matrix suite of codes from the OP and IP [11,16,17]. The first stage, STG1, starts with target or core wave function which forms the first term of the ion wave function  $\Psi_E$ . R-matrix basis set contained 14 terms for each continuum orbital. The second sum in the wavefunction expansion, Eq. (1), includes 56 possible  $(N + 1)$ –electron configurations with range of minimum and maximum occupancies as listed within parentheses of the orbitals:  $3s(0 - 2)$ ,  $3p(4 - 6)$ ,  $3d(3 - 8)$ ,  $4s(0 - 2)$ ,  $4p(0 - 3)$ , and  $4d(0 - 2)$  of Cr I. All  $SL\pi$  symmetries of the  $(e + \text{ion})$  system formed from the 40 target states coupled with an interacting electron with partial waves  $0 \leq l \leq 12$  are included.

The Hamiltonian and dipole matrices are computed by STGH and bound states are computed by STGB. The energy eigenvalues are obtained by searching the poles in the Hamiltonian. The bound states of Cr I were identified using quantum defect analysis and percentage of channel contributions to the states.

For higher resolution of resonances in photoionization and recombination,  $\sigma_{pl}$  in the near threshold energy region was resolved with a finer energy mesh, 4000 energy points upto 0.4 Ry above the ionization threshold.  $\sigma_{pl}$  at higher photoelectron energies, beyond the highest target threshold, are extrapolated as explained in [6] and were processed by the code ELEVID [13].

State-specific recombination rate coefficients for all bound states with  $n \leq 10$  are obtained from code RECOMB [13] and are added together for the total. The contributions of high- $n$  states below the target thresholds are obtained from the resonance averaged DR collision strength  $\Omega(DR)$  using code STGFDR [6].  $\Omega(DR)$  was calculated using the radiative decay rate

**Table 1**  
Terms and energies of target Cr II in the eigenfunction expansion of Cr I.

	Config.	Term	$E$ (Ry)		Config.	Term	$E$ (Ry)
1	$3d^5$	$a^6S$	0.000000	21	$3d^4(^3G)4s$	$b^2G$	0.351193
2	$3d^4(^5D)4s$	$a^6D$	0.111884	22	$3d^4(a^1G)4s$	$c^2G$	0.362337
3	$3d^4(^5D)4s$	$a^4D$	0.180686	23	$3d^5$	$c^2F$	0.362859
4	$3d^5$	$a^4G$	0.186950	24	$3d^4(^1I)4s$	$b^2I$	0.366459
5	$3d^5$	$a^4P$	0.198868	25	$3d^4(^1S)4s$	$a^2S$	0.368289
6	$3d^5$	$b^4D$	0.228178	26	$3d^4(^3D)4s$	$b^2D$	0.391238
7	$3d^4(^3P)4s$	$b^4P$	0.278180	27	$3d^5$	$b^2S$	0.403756
8	$3d^5$	$a^2I$	0.274718	28	$3d^4(^1D)4s$	$c^2D$	0.416505
9	$3d^4(^3H)4s$	$a^4H$	0.275971	29	$3d^4(^5D)4p$	$z^6F^o$	0.431548
10	$3d^4(^3F)4s$	$a^4F$	0.283983	30	$3d^5$	$d^2D$	0.431591
11	$3d^5$	$a^2D$	0.286348	31	$3d^4(^5D)4p$	$z^6P^o$	0.442268
12	$3d^5$	$a^2F$	0.295814	32	$3d^4(^5D)4p$	$z^4P^o$	0.449377
13	$3d^5$	$b^4F$	0.299333	33	$3d^4(^5D)4p$	$z^6D^o$	0.452263
14	$3d^4(^3G)4s$	$b^4G$	0.306084	34	$3d^4(^1F)4s$	$d^2F$	0.461794
15	$3d^4(^3H)4s$	$a^2H$	0.316485	35	$3d^4(^5D)4p$	$z^4F^o$	0.471936
16	$3d^4(^3P)4s$	$a^2P$	0.320071	36	$3d^5$	$d^2G$	0.476690
17	$3d^4(^3F)4s$	$b^2F$	0.324330	37	$3d^34s^2$	$c^4F$	0.488048
18	$3d^5$	$b^2H$	0.324988	38	$3d^4(^5D)4p$	$z^4D^o$	0.497945
19	$3d^5$	$a^2G$	0.329847	39	$3d^4(^3F)4s$	$d^4F$	0.500076
20	$3d^4(^3D)4s$	$c^4D$	0.349147	40	$3d^4(^3P)4s$	$c^4P$	0.503464

The optimized set of configurations for the target is,  $3s^23p^63d^5$ ,  $3s^23p^63d^44s$ ,  $3s^23p^63d^44p$ ,  $3s^23p^63d^34s^2$ ,  $3s^23p^63d^44d$ ,  $3s^23p^53d^6$ ,  $3s^23p^43d^7$ ,  $3s^23p^63d^34p^2$ ,  $3s3p^63d^54s$ ,  $3s3p^63d^54p$ ,  $3s3p^63d^44s^2$ ,  $3p^63d^7$ ,  $3s^23p^63d^34s4p$ ,  $3s^23p^63d^34s4d$ , with filled  $1s^22s^22p^6$ . The first four configurations are spectroscopic while the rest are correlation.

( $A$ -value),  $6.418886e-09 \text{ s}^{-1}$ , for the dipole allowed transition to the core ground state,  $3d^4 4p(^6P^o) - 3d^5(^6S)$ . The  $A$ -value was obtained from using the atomic structure code SUPERSTRUCTURE. The contributions from all  $n \leq \infty$  were added for the total unified  $\sigma_{RC}(E)$ ,  $\alpha_R(E)$  and  $\alpha_R(T)$  using programs RECXs and PRCOMG.

#### 4. Results and discussions

Results from detailed study of inverse processes of photoionization and electron–ion recombination of neutral Cr in LS coupling are presented. Only the septet and quintet states, relevant to total recombination, of Cr I are considered. The aim of the present work is to study general features and provide results for photoionization and electron–ion recombination of the atom with good approximation. These represent first detailed theoretical study for the state-specific and total recombination for this atom.

Due to strong electron–electron correlations it is difficult to represent this neutral atom accurately. Present calculations considers a wave function expansion which includes the ground and lowest 39 excited states, all lying within about 0.5 Ry, of Cr II. The set includes one  $^6P^o$  state for a single dipole transition of the ground state,  $3d^5(^6S) - 2d^4 4p(^6P^o)$  which can introduce a phot-excitation-of-core (PEC) resonance in photoionization cross sections. The wave function expansion, as described in the Computation section, has considerable number of configurations and hence is expected to provide good approximations for photoionization cross sections and electron–ion recombination rates in LS coupling.

Following subsections discuss energies, photoionization cross sections and recombination rates in separately.

##### 4.1. LS term energies

A total of 134 septet and quintet bound states of Cr I are obtained. The energies of the states are compared in Table 2 with those obtained from statistical averaging of fine structure levels listed in the NIST [15] compiled table (source references are listed in the website). Very good agreement is found between the calculated and measured values for the ground and many excited states. However, some large differences are also noted. The largest one being 16% for  $3d^5(^4G)4s\ a^5G$  state.

**Table 2**

Comparison of calculated LS term energies,  $E_c$ , of Cr I with the term energies,  $E_o$ , obtained from statistical averaging of observed fine structure level energies [15].

Config.	Term	$E_o$ (Ry)	$E_c$ (Ry)	Config.	Term	$E_o$ (Ry)	$E_c$ (Ry)
$3d^5(^6S)4s$	$a^7S : 1$	0.497330	0.4933077	$3d^5(^6S)4s$	$a^5S : 1$	0.428136	0.4230145
$3d^4 4s^2$	$a^5D : 1$	0.423607	0.3744548	$3d^5(^4G)4s$	$a^5G : 1$	0.310325	0.2680178
$3d^5(^4P)4s$	$a^5P : 1$	0.298251	0.2724371	$3d^5(^6S)4p$	$z^7P^o : 1$	0.283955	0.3059220
$3d^5(^4D)4s$	$b^5D : 2$	0.275963	0.2407274	$3d^4(^5D)4s4p^3P^o$	$z^7F^o : 1$	0.265572	0.2361097
$3d^5(^6S)4p$	$z^5P^o : 1$	0.253171	0.2768377	$3d^4(^5D)4s4p^3P^o$	$z^7D^o : 1$	0.245757	0.2140152
$3d^4(^5D)4s4p^3P^o$	$y^7P^o : 2$	0.243562	0.2213843	$3d^4(^5D)4s4p^3P^o$	$y^5P^o : 2$	0.227012	0.2001276
$3d^4(^5D)4s4p^3P^o$	$z^5P^o : 1$	0.214198	0.1827097	$3d^5(^4F)4s$	$a^5F : 1$	0.211423	0.1709271
$3d^4(^5D)4s4p^3P^o$	$z^5D^o : 1$	0.190646	0.1581317	$3d^6$	$c^5D : 3$	0.173848	0.1427154
$3d^5(^6S)5s$	$e^7S : 2$	0.161111	0.1574860	$3d^5(^6S)5s$	$e^5S : 2$	0.152112	0.1482581
$3d^4(^5D)4s4p^1P^o$	$y^5F^o : 2$	0.122010	0.0919476	$3d^4(^5D)4s4p^1P^o$	$x^5P^o : 3$	0.123705	0.1161119
$3d^4(^5D)4s4p^1P^o$	$y^5D^o : 2$	0.118533	0.1021285	$3d^4(^3H)4s4p^3P^o$	$z^5H^o*1$	0.112776	0.0853737
$3d^5(^6S)5p$	$x^7P^o : 3$	0.112235	0.1122970	$3d^5(^6S)4d$	$e^7D : 1$	0.112248	0.1034247
$3d^5(^4G)4p$	$z^5G^o : 1$	0.109375	0.0929636	$3d^5(^4P)4p$	$z^5S^o : 1$	0.104347	0.101653
$3d^5(^6S)4d$	$e^5D : 4$	0.095752	0.0909252	$3d^5(^6S)5p$	$w^5P^o : 4$	0.094472	0.0872249
$3d^4(a^3P)4s4p^3P^o$	$v^5P^o : 6$	0.087765	0.0538745	$3d^5(^6S)6s$	$f^7S : 3$	0.081397	0.0800004
$3d^5(^6S)6s$	$f^5S : 3$	0.078440	0.0768789	$3d^4(a^3F)4s4p^3P^o$	$w^5D^o : 3$	0.074829	0.0754354
$3d^4 4s5s$	$f^7D : 2$	0.071371	0.0677150	$3d^5(^4P)4p$	$u^5P^o : 5$	0.069609	0.0600586
$3d^4(^3D)4s5p^3P^o$	$v^5F^o : 3$	0.063215	0.0628533	$3d^5(^6S)6p$	$w^7P^o : 4$	0.062561	0.0623821
$3d^5(^6S)5d$	$g^7D : 3$	0.062611	0.0588846	$3d^5(^4G)4p$	$u^5F^o*:4$	0.060097	0.0532960
$3d^4 4s5s$	$f^5D : 5$	0.053778	0.0546972	$3d^5(^6S)7s$	$g^7S : 4$	0.049189	0.0485077
$3d^5(^6S)7s$	$g^5S : 4$	0.047879	0.0470848	$3d^5(^4D)4p$	$t^5P^o*:7$	0.044016	0.0431958
$3d^5(^4D)4p$	$s^5P^o : 6$	0.040201	0.040077	$3d^5(^6S)7p$	$7P^o*:5$	0.039949	0.0398247
$3d^5(^4D)4p$	$u^5D^o : 4$	0.036106	0.0311653	$3d^5(^6S)8s$	$h^5S : 5$	0.032259	0.0317895
$3d^5(^6S)8p$	$7P^o : 6$	0.027734	0.0276486	$3d^5(^6S)9p$	$7P^o : 7$	0.020364	0.0203233
$3d^5(^6S)10p$	$7P^o : 8$	0.015659	0.0155783	$3d^4(^3D)4s4p^3P^o$	$r^5F^o : 11$	0.013397	0.011522
$3d^4 4s4d$	$e^7G : 6$	0.010507	0.0100052	$3d^4 4s4d$	$h^7D*:8$	0.010585	0.012018

The number next to a LS state symmetry refers its position in the calculated energies of the symmetry.

\*Means incomplete set of observed levels for the state.

Spectroscopic identification of some calculated LS terms may have uncertainty since these states do not follow any well defined pattern for effective quantum numbers of a Rydberg series of states. The quantum defects of these states are perturbed by the electron–electron interactions.

Although a large set of configurations was considered to include all possible electron–electron correlations for all bound states, some high lying observed bound states listed in the NIST table are missing in the computed set. For example,  $3d^4(a^3P)4s4p^3P^o(x^5D^o)$  state at energy 0.1087 Ry was not found. Computations were repeated to find these missing states by searching the poles in the Hamiltonian with finer energy meshes and lowering the effective quantum numbers. A future computation with better optimized wave functions may result in finding these states. These indicate that a much more elaborate calculations will be needed to study this ion.

#### 4.2. Total and partial photoionization cross sections of Cr I

The *total* photoionization cross sections  $\sigma_{PI}(nLS)$ , which include contributions from all channels for ionization into various excited core states and *partial* cross sections for ionization into the core ground state are presented for all septet and quintet bound states of Cr I.

Fig. 1 presents the total photoionization cross sections  $\sigma_{PI}$  of the ground  $3d^54s^7S$  and excited  $3d^54s^5F$  states of the ground configuration. These states show existence of extensive high-peak resonances near the first ionization threshold. These represent high probabilities of both photoionization and recombination of the atom in the low energy region. The energy region has almost zero background until the background cross section is enhanced at the first excited core threshold,  $3d^44s^6D$ , which is 0.11 Ry from the ionization threshold.

Among the earlier works, Huber et al. [2] made the first measurement of resonant features of Cr I photoionization in a very small energy range, 181.9–179.3 nm (0.5–0.508 Ry) using interferometer hook method. They assigned the features belonging to the ground state. However, the measured energy range overlaps three states of Cr I,  $3d^54s(^7S)$ ,  $3d^54s(^5S)$ , and  $3d^44s^2(^5D)$  which have closely lying ionization energies at 0.497, 0.428 and 0.424 Ry, respectively. Therefore isolating these states in the experimental beam would be difficult. The present results, shown in Fig. 2, indicate that the observed features belong mainly to two excited states  $^5S$  and  $^5D$  instead of the ground state which does not show any resonance in this energy region. In the figure, the calculated cross sections were shifted slightly to match the exact ionization energies. The resonances in the cross sections can be identified through their effective quantum number  $\nu$  with respective to the target (core) states as

$$\nu = z/\sqrt{(E_r - E_c)}, \tag{15}$$

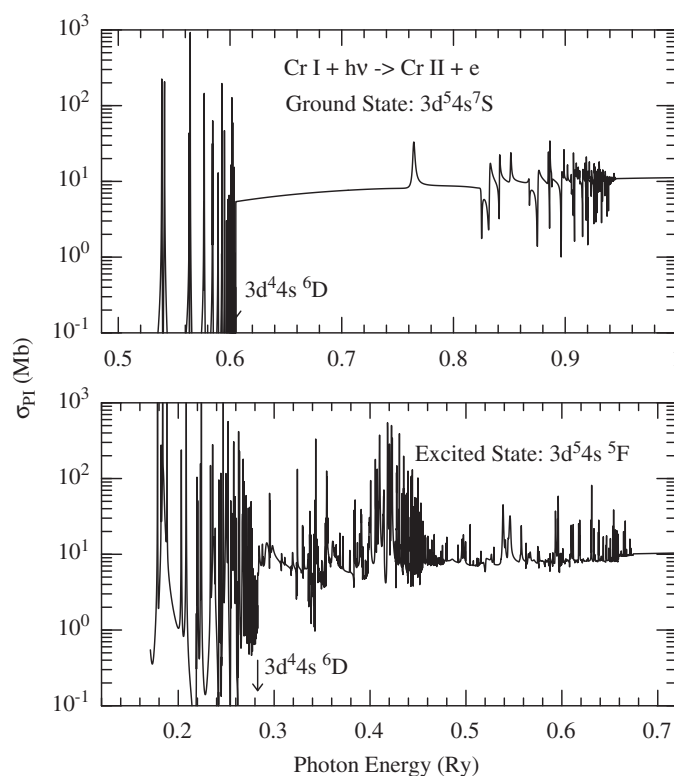


**Fig. 1.** Total photoionization cross sections  $\sigma_{PI}$  of the ground  $3d^54s^7S$  and excited  $3d^54s^5F$  states of Cr I. The ionization is enhanced at the first excited threshold  $3d^44s^6D$  state of the core (pointed by an arrow). The existence of the high-peak resonances at and near the first ionization threshold indicate high probabilities of both photoionization and recombination of the atom.

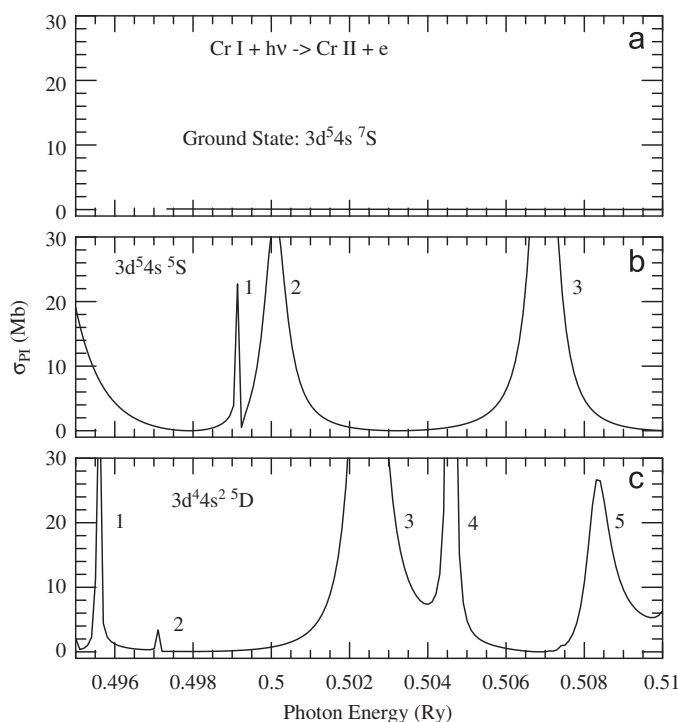


**Fig. 2.** Photoionization cross sections  $\sigma_{PI}$  of the three lowest states of Cr I, (a) ground state  $3d^6(^7S)$ , excited (b)  $3d^5 4s(^5S)$  and (c)  $3d^4 4s^2(^5D)$  states, in a small energy region below the first excited core state  $3d^4 4s(^6D)$ . Experiment carried out in this energy region showed combined features of the states [2]. While the ground state,  $^7S$ , has featureless background, the excited states exhibit resonances indicating resonant features observed in the experiment belong to the excited states. (See text for identification of resonances.)

where  $z$  is the charge of residual ion (1 for Cr I),  $E_r$  and  $E_c$  are the energies of the resonance and of the respective excited core state. The middle panel, Fig. 2(b), shows photoionization cross section of  $3d^5 4s(^5S)$  state and hence all resonances have the symmetry  $^5P^o$ . Effective quantum number of the three resonances (denoted by numbers in the figure) with respect to the first excited core state  $3d^4 4s(^6D)$  are 4.95(1), 5.01(2) and 5.50(3), respectively. Hence the possible spectroscopic identification for the first two resonances are  $3d^4 \ ^5D 4s 5f \ ^3F^o(^5P^o)$  and  $3d^4 \ ^5D 4s 5f \ ^1F^o(^5P^o)$  with about zero quantum defect ( $\mu = n - \nu$ ) for the  $5f$  electron, and for the third resonance is  $3d^4 4s 6p(^5P^o)$ , which was observed in the experiment, with about 0.5 quantum defect for the  $6p$  electron. Fig. 2(c) presents photoionization cross section of  $3d^4 4s^2(^5D)$  and hence the resonances belong to three different symmetries  $^5P^o, ^5D^o, ^5F^o$  formed from probable configuration  $3d^4 4s n p$ . For the five resonances in the panel the effective quantum numbers with respect to the first excited core state  $3d^4 4s(^6D)$  are 5.01(1), 5.10(2), 5.50(3), 5.69(4), and 6.07(5). They indicate that the third and fourth resonances are from  $3d^4 4s 6p$ , and that  $\mu$  of the first, second, and fifth resonances are significantly perturbed. These may also belong to  $3d^3 4s^2 n f$  since the list of core configurations includes the configuration  $3d^3 4s^2$ . The third and fourth resonances were observed by Huber et al. The present resonances are broad due to LS coupling approximation while a fine structure calculations could have shown narrower resonances as observed in the experiment.

The compiled energy table by the NIST [15] lists one septet and several quintet autoionizing states which can appear as resonances in photoionization cross sections. To illustrate these resonances, Fig. 3 presents photoionization cross sections of  $3d^4 4p^2 \ ^7F$  state in panel (a) and of  $3d^5 4p(^5P^o)$  state in panel (b). The identified resonances (pointed by arrows in the figure) correspond to autoionizing state  $3d^4 4p^2 \ ^7F$  in  $\sigma_{PI}$  of  $^7F^o$  state in panel (a) and  $3d^4 4s 5s^5 D, 3d^4 4s 5s^5 P$  states in  $\sigma_{PI}$  of  $^5P^o$  state in panel (b). The observed energy position of  $^7F$  state is 0.0712 Ry above the ionization threshold while the calculated energy position is 0.0734 Ry (0.1352 Ry photon energy). The observed energies of the autoionizing states  $^5D$  and  $^5P$  are at 0.0037 and 0.0652 Ry above the ionization threshold while the calculated positions are at 0.0032 and 0.0677 Ry. (The fine structure levels in the NIST table were averaged statistically to obtain their LS term energies.)

The excited states with a valence electron exhibit characteristic features in photoionization cross sections. These are illustrated in Fig. 4 presenting total photoionization cross sections of five excited states of Cr I:  $3s^2 3p^6 3d^5 n p(^7P^o)$ , with  $5 \leq n \leq 9$ . All these states show, similar to the ground state, in the background cross sections an enhancement at an energy 0.11 Ry above the ionization threshold corresponding to the first excited state,  $3s^2 3p^6 3d^4 4s(^6D)$  of the core Cr II. The enhancement becomes less noticeable with higher excited states.

The most prominent feature in Fig. 4 is the presence of a wide and high-peak PEC resonance at the photon energy, 0.44 Ry, the core excitation energy for the dipole allowed transition,  $3s^2 3p^6 3d^5(^6S) - 3s^2 3p^6 3d^4 4p(^6P^o)$ . The PEC resonance spanning over a large energy range has enhanced the background considerably. This explains that the correlations of channels with excited core states contribute considerably to photoionization contradicting the usual assumption of weaker couplings for excited states. PEC resonances were first explained and named by Seaton in [18]. A PEC resonance is formed

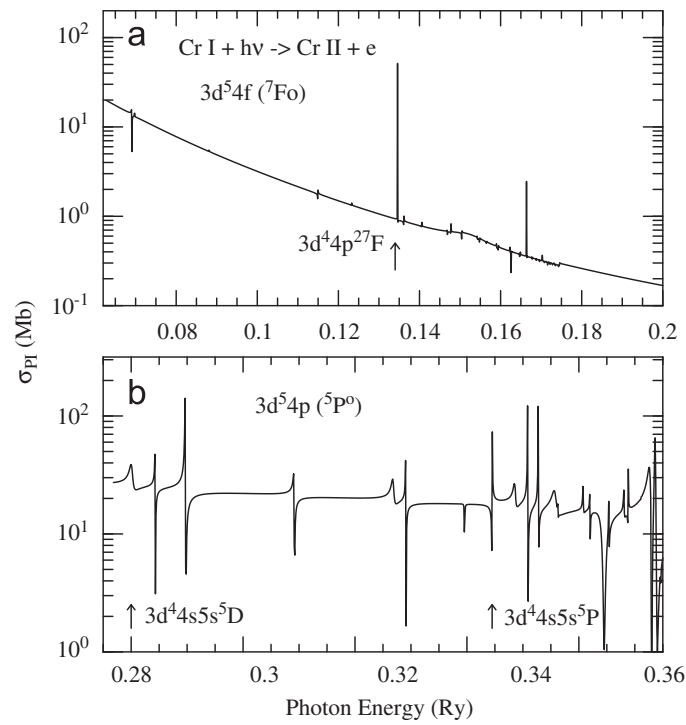


**Fig. 3.** Photoionization cross sections  $\sigma_{PI}$  of (a)  $3d^5 4f ({}^7F_0)$  and (b)  $3d^5 4p ({}^5P_0)$  states of Cr I illustrating resonances due to observed autoionizing states [15] (pointed by arrows).

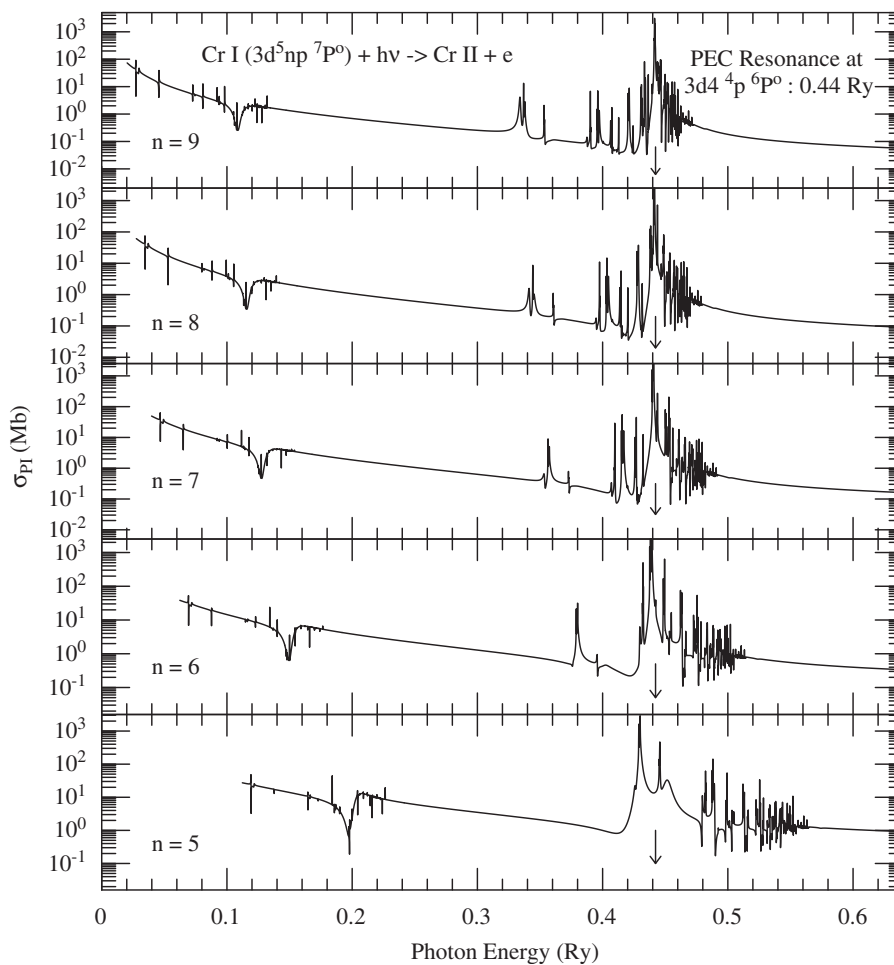


**Fig. 4.** Total photoionization cross sections,  $\sigma_{PI}$ , of excited Rydberg series of states  $3s^2 3p^6 3d^5 np ({}^7P^o)$ , with  $5 \leq n \leq 9$ , of Cr I. At 0.44 Ry photon energy is the prominent PEC resonance (pointed by arrow) formed due to dipole allowed transition by the core ground state to excited ( ${}^6S-{}^6P^o$ ) state at 0.44 Ry.

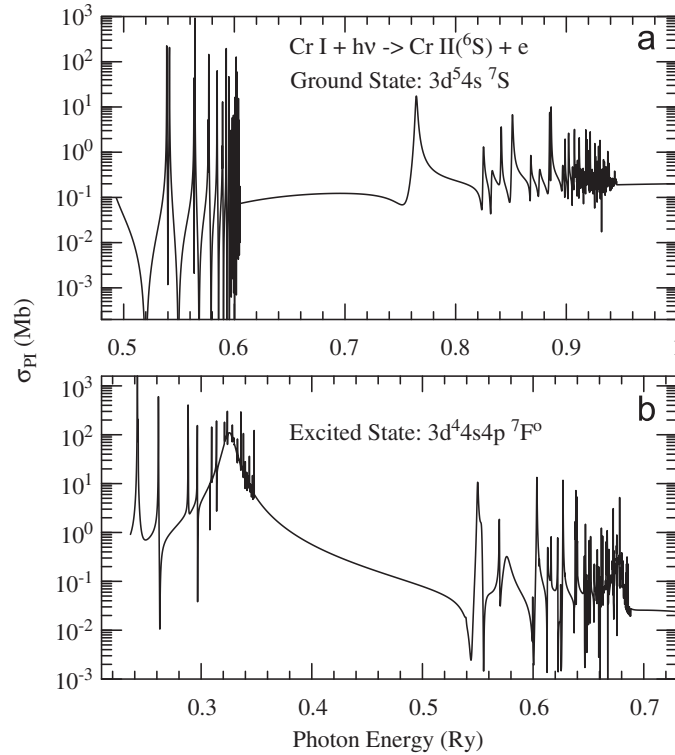


**Fig. 5.** Partial photoionization cross sections for the ground  $3d^5 4s(^7S)$  and excited  $3d^4 4s 4p ^7F^0$  states of Cr I. The background is lower as these cross sections do not include contributions for ionization into excited core states.  $3d^4 4s 4p ^7F^0$  is a dominant contributor to total recombination rate due to resonances at the threshold.

when the ion absorbs a photon for a dipole allowed core excitation from the ground state during which the outer electron remains temporarily attached to a highly excited level and autoionizes as the core ultimately drops to the ground state. The process is inverse to dielectronic recombination and is manifested in a large resonance at the excitation threshold energy.

Compared to the total, *partial* photoionization cross sections,  $\sigma_{PI}(g, nLS)$ , for ionization into the ground  $3s^2 3p^6 3d^5(^6S)$  state of the residual ion Cr II, have lower background. Since partial photoionization does not include contributions for ionization into excited core states, the background is lower and lacks the corresponding resonances. Fig. 5 presents partial cross sections for the ground state and one excited state,  $3d^4 4s 4p ^7F^0$ , of Cr I. The partial cross sections are needed to calculate the recombination rates of the ion. Comparing the total and partial cross sections of the ground state, in the top panel of Figs. 1 and 5, respectively, a clear difference can be seen. The enhanced background of the total (Fig. 1) is about 5 Mb while of the partial is about 0.1 Mb (Fig. 5). The bottom panel of Fig. 5 shows cross sections of excited state  $3d^4 4s 4p ^7F^0$ . It is one of the dominant contributor to the total recombination rate because of high-peak resonances right at the ionization threshold and existence of a large resonance, belonging to  $3d^4 4p(^6P^0)nl$  Rydberg series, around 0.32 Ry.

#### 4.3. Total and state-specific recombination rate coefficients

Structures of both total and state-specific recombination rate coefficients of Cr I are studied. The state-specific recombination rates  $\alpha_R(nLS)$  for 134 bound states with  $n \leq 10$  and  $0 \leq l \leq 9$  are obtained for the first time.

The rates of recombination into various individual states vary with temperature depending on the positions of resonances and background features in the photoionization cross sections. Illustrative examples of  $\alpha_R(nLS)$  are given in Fig. 6 for a number of states. Except the ground state, other states in the figure are dominant contributors to the total recombination rate at various temperatures. Rates for these states are tabulated in Table 3. As can be seen, ground state is not the most dominant contributor to the total recombination because of its low background near threshold and relatively low-peak resonances in the higher energy region. Although low energy high-peak resonances exist in photoionization cross sections, they are not right at the ionization threshold and contributions from high energy resonances are damped out by the exponential factor,  $\exp(-E/kT)$ , in the recombination rate integral. Compared to the ground state,  $3d^5 4p(^7P^0)$  state is an important contributor above 11,000 K because of its high DR peak. Most of the states show one high temperature DR peak.  $\alpha_R(nLS)$  are needed for determination of level populations and formation of cascade matrices.

The features of the total unified recombination rate coefficients,  $\alpha_R(T)$ , for Cr I are presented in Fig. 7 and the numerical values are presented in Table 4. The present  $\alpha_R(T)$  shows a characteristic rapid rise with decreasing temperature caused by very low energy recombination to the infinite number of high- $n$  states, mainly via RR, which is followed by one low temperature DR peak at about 630 K, and one at higher temperature, 40,000 K, after which the rate decays smoothly. Cr I

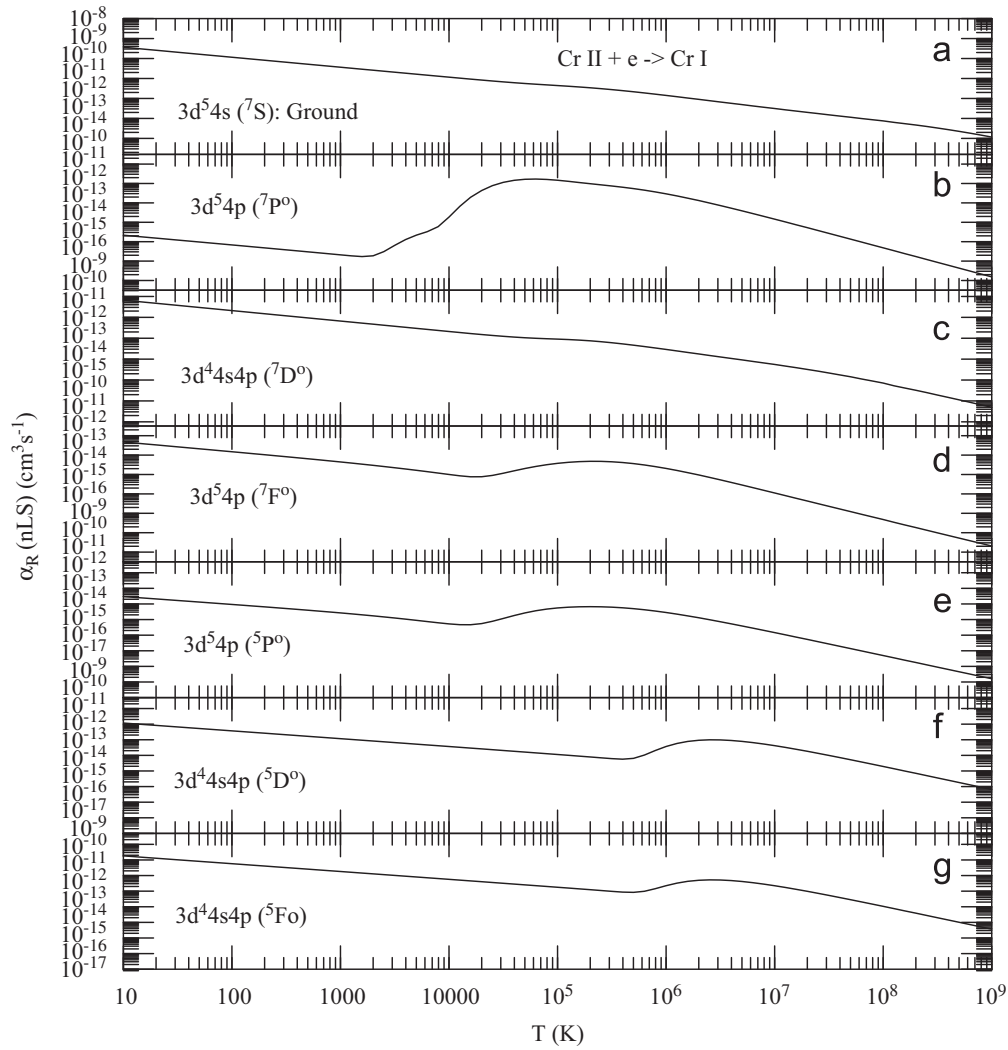


**Fig. 6.** Total (RR + DR) state-specific recombination rate coefficients  $\alpha_{R}(nLS)$  of Cr I in a wide temperature range. The states are specified in each panel. Recombination rate of each state varies with temperature depending on the dominant features in the state-specific photoionization.

**Table 3**

State-specific recombination rate coefficients  $\alpha_{R}(nSL\pi)$  of the ground and several dominant excited states of Cr I.

$\log_{10} T$	$\alpha_{R}(nSL\pi)$ ( $\text{cm}^3/\text{s}$ )						
BE(Ry) =	$3d^5 4s^7 S$	$3d^5 4p^7 P^0$	$3d^4 4s 4p^7 D^0$	$3d^4 4s 4p^7 F^0$	$3d^5 4p^5 P^0$	$3d^4 4s 4p^5 D^0$	$3d^4 4s 4p^5 F^0$
1.0	1.13E-14	3.38E-12	7.59E-13	1.75E-13	2.16E-12	2.23E-14	2.12E-14
1.1	1.01E-14	3.01E-12	6.76E-13	1.56E-13	1.93E-12	1.98E-14	1.89E-14
1.2	8.96E-15	2.68E-12	6.02E-13	1.40E-13	1.72E-12	1.76E-14	1.69E-14
1.3	7.96E-15	2.39E-12	5.36E-13	1.25E-13	1.53E-12	1.56E-14	1.52E-14
1.4	7.07E-15	2.13E-12	4.78E-13	1.12E-13	1.37E-12	1.38E-14	1.36E-14
1.5	6.27E-15	1.90E-12	4.26E-13	1.00E-13	1.22E-12	1.22E-14	1.23E-14
1.6	5.55E-15	1.69E-12	3.79E-13	9.03E-14	1.09E-12	1.07E-14	1.11E-14
1.7	4.91E-15	1.51E-12	3.37E-13	8.15E-14	9.72E-13	9.38E-15	1.01E-14
1.8	4.33E-15	1.34E-12	3.00E-13	7.39E-14	8.69E-13	8.21E-15	9.24E-15
1.9	3.80E-15	1.20E-12	2.68E-13	6.84E-14	7.77E-13	7.17E-15	8.76E-15
2.0	3.33E-15	1.07E-12	2.39E-13	7.04E-14	6.97E-13	6.30E-15	9.87E-15
2.1	2.91E-15	9.48E-13	2.17E-13	1.02E-13	6.26E-13	5.84E-15	1.73E-14
2.2	2.53E-15	8.44E-13	2.08E-13	2.10E-13	5.62E-13	6.58E-15	4.13E-14
2.3	2.18E-15	7.53E-13	2.24E-13	4.49E-13	5.05E-13	1.02E-14	9.33E-14
2.4	1.87E-15	6.74E-13	2.71E-13	8.29E-13	4.52E-13	1.88E-14	1.76E-13
2.5	1.60E-15	6.06E-13	3.42E-13	1.29E-12	4.03E-13	3.40E-14	2.77E-13
2.6	1.35E-15	5.48E-13	4.18E-13	1.72E-12	3.59E-13	5.62E-14	3.75E-13
2.7	1.13E-15	4.97E-13	4.78E-13	2.02E-12	3.19E-13	8.34E-14	4.47E-13
2.8	9.36E-16	4.51E-13	5.06E-13	2.15E-12	2.83E-13	1.11E-13	4.81E-13

Table 3 (continued)

$\log_{10} T$	$\alpha_R(nS\pi)$ (cm <sup>3</sup> /s)						
	$3d^5 4s^7 S$	$3d^5 4p^7 P^0$	$3d^4 4s4p^7 D^0$	$3d^4 4s4p^7 F^0$	$3d^5 4p^5 P^0$	$3d^4 4s4p^5 D^0$	$3d^4 4s4p^5 F^0$
BE(Ry) =	-4.93E-01	-3.06E-01	-2.14E-01	-2.36E-01	-2.77E-01	-1.58E-01	-1.83E-01
2.9	7.84E-16	4.07E-13	5.00E-13	2.10E-12	2.50E-13	1.34E-13	4.78E-13
3.0	7.21E-16	3.66E-13	4.65E-13	1.93E-12	2.22E-13	1.49E-13	4.46E-13
3.1	8.47E-16	3.26E-13	4.13E-13	1.68E-12	1.96E-13	1.52E-13	3.96E-13
3.2	1.29E-15	2.89E-13	3.53E-13	1.41E-12	1.73E-13	1.46E-13	3.41E-13
3.3	2.13E-15	2.55E-13	2.94E-13	1.15E-12	1.54E-13	1.34E-13	2.88E-13
3.4	3.34E-15	2.24E-13	2.40E-13	9.16E-13	1.36E-13	1.19E-13	2.43E-13
3.5	4.73E-15	1.97E-13	1.95E-13	7.27E-13	1.21E-13	1.03E-13	2.05E-13
3.6	6.04E-15	1.74E-13	1.58E-13	5.78E-13	1.07E-13	8.93E-14	1.74E-13
3.7	7.02E-15	1.54E-13	1.29E-13	4.65E-13	9.54E-14	7.69E-14	1.48E-13
3.8	7.51E-15	1.39E-13	1.05E-13	3.77E-13	8.46E-14	6.58E-14	1.24E-13
3.9	7.51E-15	1.26E-13	8.58E-14	3.06E-13	7.49E-14	5.59E-14	1.03E-13
4.0	7.11E-15	1.14E-13	6.96E-14	2.48E-13	6.61E-14	4.68E-14	8.49E-14
4.1	6.47E-15	1.04E-13	5.59E-14	1.99E-13	5.81E-14	3.86E-14	6.85E-14
4.2	5.74E-15	9.40E-14	4.44E-14	1.58E-13	5.09E-14	3.14E-14	5.43E-14
4.3	5.02E-15	8.47E-14	3.49E-14	1.24E-13	4.46E-14	2.52E-14	4.25E-14
4.4	4.38E-15	7.62E-14	2.71E-14	9.56E-14	3.90E-14	2.02E-14	3.29E-14
4.5	3.84E-15	6.84E-14	2.08E-14	7.29E-14	3.43E-14	1.63E-14	2.53E-14
4.6	3.37E-15	6.07E-14	1.59E-14	5.50E-14	2.99E-14	1.32E-14	1.94E-14
4.7	3.00E-15	5.40E-14	1.20E-14	4.11E-14	2.61E-14	1.08E-14	1.48E-14
4.8	2.69E-15	4.76E-14	8.98E-15	3.05E-14	2.27E-14	8.97E-15	1.13E-14
4.9	2.40E-15	4.10E-14	6.68E-15	2.25E-14	1.93E-14	7.32E-15	8.56E-15
5.0	2.14E-15	3.51E-14	4.93E-15	1.64E-14	1.63E-14	5.99E-15	6.49E-15
5.1	1.89E-15	2.94E-14	3.62E-15	1.20E-14	1.34E-14	4.79E-15	4.88E-15
5.2	1.66E-15	2.43E-14	2.64E-15	8.69E-15	1.09E-14	3.78E-15	3.65E-15
5.3	1.44E-15	2.00E-14	1.92E-15	6.28E-15	8.74E-15	2.96E-15	2.72E-15
5.4	1.23E-15	1.62E-14	1.39E-15	4.52E-15	6.89E-15	2.27E-15	2.01E-15
5.5	1.05E-15	1.31E-14	1.00E-15	3.25E-15	5.41E-15	1.74E-15	1.48E-15
5.6	8.62E-16	1.04E-14	7.22E-16	2.33E-15	4.12E-15	1.28E-15	1.07E-15
5.7	7.07E-16	8.27E-15	5.19E-16	1.66E-15	3.17E-15	9.58E-16	7.85E-16
5.8	5.71E-16	6.59E-15	3.72E-16	1.19E-15	2.43E-15	7.15E-16	5.73E-16
5.9	4.44E-16	5.03E-15	2.66E-16	8.45E-16	1.75E-15	4.83E-16	4.00E-16
6.0	3.48E-16	3.96E-15	1.90E-16	6.02E-16	1.32E-15	3.51E-16	2.87E-16
6.1	2.70E-16	3.11E-15	1.36E-16	4.28E-16	9.93E-16	2.55E-16	2.07E-16
6.2	2.06E-16	2.42E-15	9.73E-17	3.04E-16	7.36E-16	1.83E-16	1.48E-16
6.3	1.57E-16	1.88E-15	6.95E-17	2.16E-16	5.50E-16	1.31E-16	1.06E-16
6.4	1.19E-16	1.46E-15	4.97E-17	1.54E-16	4.08E-16	9.47E-17	7.58E-17
6.5	8.90E-17	1.12E-15	3.55E-17	1.09E-16	3.03E-16	6.84E-17	5.44E-17
6.6	6.65E-17	8.64E-16	2.53E-17	7.75E-17	2.25E-16	4.94E-17	3.90E-17
6.7	4.94E-17	6.61E-16	1.81E-17	5.50E-17	1.67E-16	3.57E-17	2.80E-17
6.8	3.67E-17	5.04E-16	1.29E-17	3.90E-17	1.24E-16	2.59E-17	2.01E-17
6.9	2.71E-17	3.83E-16	9.22E-18	2.77E-17	9.14E-17	1.88E-17	1.44E-17
7.0	2.00E-17	2.90E-16	6.58E-18	1.97E-17	6.77E-17	1.37E-17	1.04E-17
7.1	1.48E-17	2.19E-16	4.70E-18	1.40E-17	5.02E-17	1.01E-17	7.52E-18
7.2	1.09E-17	1.65E-16	3.36E-18	9.94E-18	3.72E-17	7.45E-18	5.47E-18
7.3	7.99E-18	1.25E-16	2.40E-18	7.07E-18	2.76E-17	5.52E-18	3.96E-18
7.4	5.88E-18	9.36E-17	1.71E-18	5.03E-18	2.05E-17	4.17E-18	2.92E-18
7.5	4.32E-18	7.03E-17	1.23E-18	3.58E-18	1.53E-17	3.15E-18	2.14E-18
7.6	3.18E-18	5.28E-17	8.77E-19	2.56E-18	1.15E-17	2.40E-18	1.56E-18
7.7	2.34E-18	3.96E-17	6.28E-19	1.83E-18	8.61E-18	1.85E-18	1.15E-18
7.8	1.73E-18	2.97E-17	4.50E-19	1.31E-18	6.50E-18	1.45E-18	8.80E-19
7.9	1.28E-18	2.23E-17	3.23E-19	9.37E-19	4.94E-18	1.15E-18	6.65E-19
8.0	9.48E-19	1.68E-17	2.32E-19	6.74E-19	3.78E-18	9.26E-19	5.12E-19
8.1	7.05E-19	1.27E-17	1.67E-19	4.86E-19	2.91E-18	7.62E-19	4.11E-19
8.2	5.26E-19	9.61E-18	1.21E-19	3.52E-19	2.26E-18	6.16E-19	3.09E-19
8.3	3.95E-19	7.31E-18	8.75E-20	2.57E-19	1.77E-18	5.14E-19	2.51E-19
8.4	2.98E-19	5.58E-18	6.36E-20	1.88E-19	1.40E-18	4.32E-19	1.99E-19
8.5	2.27E-19	4.29E-18	4.64E-20	1.39E-19	1.12E-18	3.67E-19	1.62E-19
8.6	1.74E-19	3.32E-18	3.40E-20	1.03E-19	9.04E-19	3.14E-19	1.34E-19
8.7	1.34E-19	2.59E-18	2.51E-20	7.76E-20	7.39E-19	2.71E-19	1.12E-19
8.8	1.05E-19	2.04E-18	1.87E-20	5.89E-20	6.10E-19	2.35E-19	9.47E-20
8.9	8.24E-20	1.61E-18	1.40E-20	4.52E-20	5.08E-19	2.05E-19	8.06E-20
9.0	6.56E-20	1.29E-18	1.06E-20	3.51E-20	4.27E-19	1.79E-19	6.91E-20

lines, in abundance of 30 times more than the determined value of its abundance toward  $\zeta$  Oph, found in low temperature ( $\leq 900$  K) interstellar medium toward HD72127AB [1]. Present total rate at low temperature support the findings of Welty et al. [1].

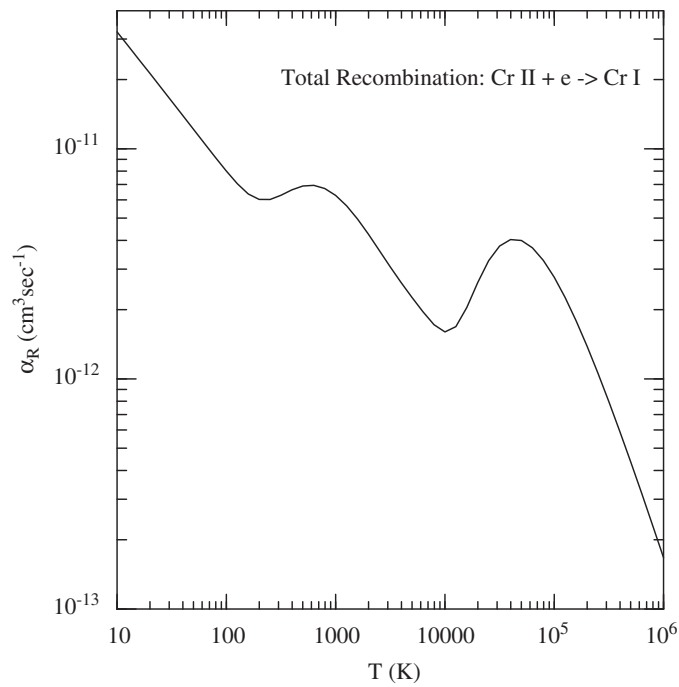


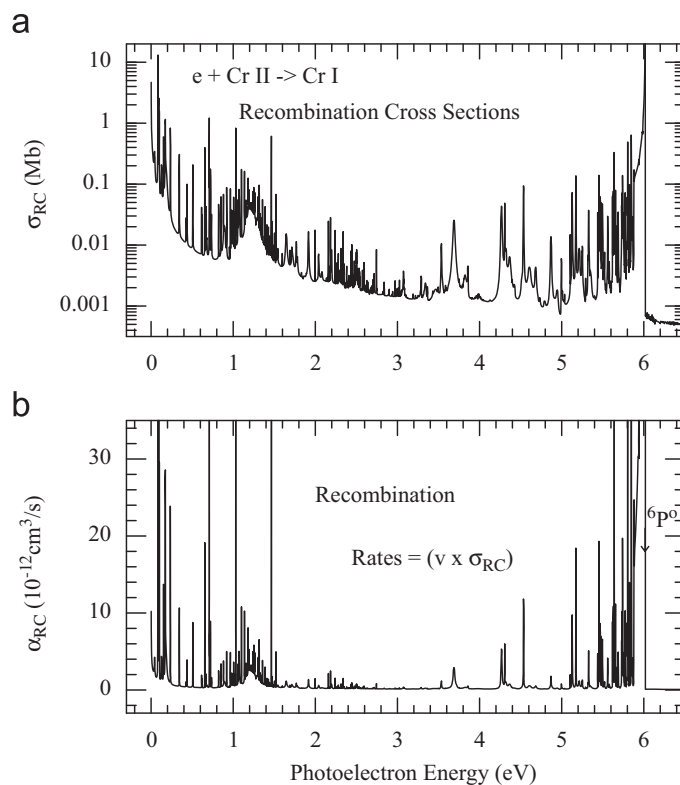
Fig. 7. Total (RR + DR) electron-ion recombination rate coefficients  $\alpha_{RC}(T)$  of Cr I.

Table 4

Total recombination rate coefficients,  $\alpha_R(T)$  for ( $e + \text{Cr II} \rightarrow \text{Cr I}$ ).

$\log T$ (K)	$\alpha_R$ ( $\text{cm}^3 \text{s}^{-1}$ )	$\log T$ (K)	$\alpha_R$ ( $\text{cm}^3 \text{s}^{-1}$ )	$\log T$ (K)	$\alpha_R$ ( $\text{cm}^3 \text{s}^{-1}$ )
1.0	3.22E-11	3.7	2.26E-12	6.4	4.47E-14
1.1	2.81E-11	3.8	1.96E-12	6.5	3.20E-14
1.2	2.44E-11	3.9	1.72E-12	6.6	2.29E-14
1.3	2.13E-11	4.0	1.60E-12	6.7	1.64E-14
1.4	1.85E-11	4.1	1.69E-12	6.8	1.17E-14
1.5	1.61E-11	4.2	2.04E-12	6.9	8.35E-15
1.6	1.40E-11	4.3	2.62E-12	7.0	5.96E-15
1.7	1.21E-11	4.4	3.27E-12	7.1	4.26E-15
1.8	1.05E-11	4.5	3.78E-12	7.2	3.04E-15
1.9	9.17E-12	4.6	4.03E-12	7.3	2.17E-15
2.0	8.00E-12	4.7	4.00E-12	7.4	1.55E-15
2.1	7.06E-12	4.8	3.71E-12	7.5	1.11E-15
2.2	6.37E-12	4.9	3.27E-12	7.6	7.92E-16
2.3	6.03E-12	5.0	2.77E-12	7.7	5.66E-16
2.4	6.02E-12	5.1	2.26E-12	7.8	4.06E-16
2.5	6.28E-12	5.2	1.79E-12	7.9	2.91E-16
2.6	6.63E-12	5.3	1.39E-12	8.0	2.09E-16
2.7	6.89E-12	5.4	1.06E-12	8.1	1.50E-16
2.8	6.94E-12	5.5	7.96E-13	8.2	1.08E-16
2.9	6.72E-12	5.6	5.91E-13	8.3	7.85E-17
3.0	6.27E-12	5.7	4.35E-13	8.4	5.70E-17
3.1	5.66E-12	5.8	3.19E-13	8.5	4.16E-17
3.2	4.95E-12	5.9	2.31E-13	8.6	3.05E-17
3.3	4.25E-12	6.0	1.67E-13	8.7	2.25E-17
3.4	3.61E-12	6.1	1.21E-13	8.8	1.67E-17
3.5	3.07E-12	6.2	8.68E-14	8.9	1.25E-17
3.6	2.62E-12	6.3	6.24E-14	9.0	9.48E-18

The present state-specific and total recombination rates of Cr I should be accurate for most of the temperature range except at very low and very high temperatures. Low temperature rates are sensitive to resolution of resonances and their positions at and very near to the ionization threshold. A slight shift in one resonance position can introduce a significant change in the rates. At higher temperature detailed features are damped out by the exponential factor in the  $\alpha_R(nLS)$  integral and hence some shift in resonant positions do not affect the rates. The present calculations do not include core



**Fig. 8.** Unified total (a) recombination cross section  $\sigma_{RC}(E)$  and (b) recombination rate coefficients  $\alpha_{RC}(E)$  with photoelectron energy for ( $e + \text{Cr II} \rightarrow \text{Cr I}$ ). Arrow in (b) points converging threshold  $3d^4 4p(^6P^o)$  where DR rate peaks and then drops to zero due to core excitation.

excitations to very high lying states, and hence resonant contributions due to these excitations are not included. The high temperature rates are probably underestimated. Based on the accuracy of the R-matrix method, energy comparison, and inclusion of interference effects, these rates are expected to be accurate within 50% for most of the temperature range.

Total recombination rate coefficient with photoelectron energy,  $\alpha_R(E)$ , of ( $e + \text{Cr II} \rightarrow \text{Cr I}$ ) can reveal detailed resonant structures in recombination spectra. These structures can be measured in storage rings. Fig. 8 presents unified  $\alpha_R(E)$  going up to  $3d^4 4p(^6P^o)$  threshold of Cr II. Panel (a) presents the total recombination cross sections  $\sigma_{RC}(E)$  and (b) presents the total recombination rate with photoelectron energy. The arrow in Fig. 8b points the excited core threshold  $3d^4 4p(^6P^o)$  where DR peaks as autoionizing resonances becomes narrower and denser and then drops almost to zero due to core excitation.

## 5. Conclusion

Photoionization and electron–ion recombination of ( $h\nu + \text{Cr I} \leftrightarrow e + \text{Cr II}$ ) are studied in detail with features. Prominent resonant feature due to a PEC resonance, manifested by the core excitation, at the photon energy 0.44 Ry is seen for the first time. Resonant structures and other features in state-specific and total recombination rates for Cr I have been obtained. The results should provide sufficiently accurate values for various modelings and understanding the radiative processes of this species.

The present computations have been carried out in LS coupling, but using a large wave function expansion. Efforts have been made to incorporate sufficient configuration interactions. However, some high lying states have not been found. Quantum defects of states are perturbed. For high precision features, these processes should be studied with inclusion of relativistic effects, with a larger wave function expansion, and more configurations. The core, Cr II, has many closely lying energy levels which will require a computationally challenging large scale relativistic calculations.

Files for photoionization cross sections, and total and state-specific recombination rates are available electronically from NORAD website at: [www.astronomy.ohio-state.edu/~nahar/nahar\\_radiativeatomicdata](http://www.astronomy.ohio-state.edu/~nahar/nahar_radiativeatomicdata)

## Acknowledgments

This work was partially supported by the NASA Astronomy and Physics Research Analysis Program. The computational work was carried out on Cray machines at the Ohio Supercomputer Center in Columbus Ohio.

## References

- [1] Welty DE, Simon T, Hobbs LM. Spatial and temporal variations in interstellar absorption toward HD 72127AB. *Mon Not R Ast Soc* 2008;388:323–34.
- [2] Huber MCE, Sandeman RJ, Tubbs EF. The spectrum of Cr I between 179.8 and 200 nm wavelengths, absorption cross sections, and oscillator strengths. *Proc R Soc Lond A* 1974;342:431–8.
- [3] Cooper JW, Clark CW, Cromer CL, Lucatorto TB. Marked differences in the 3p photoabsorption between the Cr and Mn<sup>+</sup> isoelectronic pair: reason for the unique structure observed in Cr. *Phys Rev A* 1989;39:6074–7.
- [4] Dolmatov VK. Marked difference in the 4s photoionization between the Cr(4s<sup>7</sup>S<sub>3</sub>) and Cr\*(4s<sup>5</sup>S<sub>2</sub>) atoms. *J Phys B* 1990;23:L625–8.
- [5] Nahar SN, Pradhan AK. Electron–ion recombination in the close-coupling approximation. *Phys Rev A* 1992;45:7887–93.
- [6] Nahar SN, Pradhan AK. Unified treatment of electron–ion recombination in the close-coupling approximation. *Phys Rev A* 1994;49:1816–35.
- [7] The Opacity Project Team. The opacity project, vols. 1–2. Institute of Physics Publishing; 1995–1996.
- [8] Hummer DG, Berrington KA, Eissner W, Pradhan AK, Saraph HE, Tully JA. Atomic data from the IRON project. 1: goals and methods. *Astron Astrophys* 2003;279:298–309.
- [9] Nahar SN. Atomic data from the iron project LXI. Radiative E1, E2, E3, and M1 transition probabilities for Fe IV. *Astron Astrophys* 2006;448:779–85.
- [10] Seaton MJ. Atomic data for opacity calculations. I. General description. *J Phys B* 1987;20:6363–78.
- [11] Berrington KA, Burke PG, Butler K, Seaton MJ, Storey PJ, Taylor KT, et al. Atomic data for opacity calculations. II. Computational methods. *J Phys B* 1987;20:6379–97.
- [12] Bell RH, Seaton MJ. Dielectronic recombination: I. General theory. *J Phys B* 1985;18:1589–629.
- [13] Nahar SN. Total electron–ion recombination of Fe III. *Phys Rev A* 1996;53:2417–24.
- [14] Eissner W, Jones M, Nussbaumer H. Techniques for the calculation of atomic structures and radiative data including relativistic corrections. *Comput Phys Commun* 1974;8:270–306.
- [15] Ralchenko Y, Kramida AE, Reader J, NIST ASD Team; 2008 (<http://physics.nist.gov/PhysRefData/ASD/index.html>).
- [16] Berrington KA, Eissner W, Norrington PH. RMATRIX1: Belfast atomic R-matrix codes. *Comput Phys Commun* 1995;92:290–420.
- [17] Nahar SN, Pradhan AK. Unified electron–ion recombination rate coefficients of silicon and sulfur ions. *ApJ* 1995;447:966–79.
- [18] Yu Y, Seaton MJ. Atomic data for opacity calculations. IV. Photoionisation cross sections for C II. *J Phys B* 1987;20:6409–29.